Behavior of Concrete-Faced Rockfill Dams during Initial Impoundment

Min-Woo Seo[1]; Ik Soo Ha[2]; Yong-Seong Kim[3]; and Scott M. Olson, Ph.D., P.E., M.ASCE[4]

Abstract: Centrifuge tests to investigate the behavior during initial reservoir filling of a concrete faced rockfill dam (CFRD) with face slab stiffnesses that vary by a factor of about two are described. The two centrifuge models exhibited similar deformations at the crest and along the face slab, with crest settlements averaging 0.19H (%) and maximum face slab deformations averaging 0.88H (%). The centrifuge test results suggest that the face slab stiffness had little effect on deformations, at least for the range of stiffnesses examined here. A parametric study of transition (supporting) zone stiffness was performed using a numerical model calibrated using the centrifuge results. The numerical results indicated that face slab deformation is more influenced by transition zone stiffness than face slab stiffness, supporting the centrifuge results. Deformation measurements for 25 in-service CFRDs (including six Korean CFRDs—one of which was used as the basis for the centrifuge model dam) are presented and compared with the experimental and numerical results. The centrifuge experiments exhibited crest settlements similar to the Korean CFRDs; however, the centrifuge models exhibited considerably larger maximum face slab deflections. The larger values measured in the centrifuge tests likely resulted from some experimental limitations. These limitations, as well as suggestions for improving future centrifuge studies of CFRDs, are discussed.

DOI: 10.1061/(ASCE)GT.1943-5606.0000021

CE Database subject headings: Dams, rockfill; Reservoirs; Concrete; Slabs; Measurements; Centrifuge models.

Introduction

Concrete-faced rockfill dams (CFRDs) are becoming a widely used type of rockfill dam, with recent CFRDs including Xingo Dam in Brazil, Tianshenqiao Dam in China, and Daegok Dam in Korea. CFRDs offer a number of advantages over other earthen and rockfill dam types, often involving simpler detailing and construction, shorter construction periods, and inherent resistance to earthquake loading. These advantages can result in considerable cost savings in design, construction, and maintenance. CFRDs have been constructed to heights exceeding 150 m (Hunter and Fell 2003; Xing et al. 2006), and numerous high CFRDs are being constructed and planned in China to meet increasing power and water demand (Jiang and Cao 1993; Jiang and Zhao 2000; Hou et al. 2004).

Concrete-faced rockfill dams consist of a main rockfill zone, a sub rockfill zone, a transition (or supporting) zone, and an impermeable zone created by a concrete face slab (Fig. 1). Although numerous CFRDs have been constructed and managed successfully (Pinto and Marques 1998), in many cases the design and construction of the CFRD were based primarily on precedent and engineering judgment (Cooke 1984; Özkuzukiran et al. 2006). In some cases, the lack of design guidelines and construction oversight has resulted in the use of lower permeable rockfill (i.e., silty or clayey gravel); weak, crushable rockfill materials; poor cutoff measures where CFRDs are founded on alluvium or fractured bedrock; and poor detailing (e.g., poor plinth design). These problems have led to the poor performance of some CFRDs, which commonly involve large settlements, severe cracking in the concrete face slab, and excessive leakage (Zhang and Hu 1994, Hunter and Fell 2003; and Xing et al. 2006).

Numerous techniques have been employed to evaluate CFRD behavior or to demonstrate the feasibility of a certain method used in CFRD construction, including field measurements, 1g model tests, numerical/finite-element (FE) analytical methods, and centrifuge experiments. Of course, field measurements critically depend on the instrument used to obtain the measurement, the care with which the selected instrument is employed, as well as the local field conditions and rockfill materials used for dam construction. Nevertheless, valuable field measurements of CFRD performance have been made, as discussed subsequently. Although some 1g model tests have been performed, these tests cannot simulate field stress conditions, which dominate the overall behavior, and therefore 1g model tests generally have limited usefulness in predicting CFRD performance. Many investigators and designers have performed numerical analyses of CFRDs; however the results are of unknown validity unless the numerical models are calibrated using measured field performance.

To overcome the limitations of these approaches, some investigators have performed centrifuge experiments on scaled dams. Until recently, most of these centrifuge experiments have been performed on model earthen or central clay core rockfill dams (e.g., Al-Hussaini et al. 1981; Mikasa et al. 1981; Rechard and Sutherland 1984; Fahey and Katagiri 1994; Zhang and Hu 1994; Koushige et al. 1995). The results of these centrifuge experiments

[1]Postdoctoral Research Associate, Dept. of Civil and Environmental Engineering, Univ. of Illinois at Urbana-Champaign, Urbana, IL 61801.

[2]Senior Researcher, Korea Water Resources Corporation, Daejeon, 306-711 Korea.

[3]Assistant Professor, Dept. of Agricultural Engineering, Kangwon National Univ., Gangwon-do, 200-701 Korea.

[4]Assistant Professor, Dept. of Civil and Environmental Engineering, Univ. of Illinois at Urbana-Champaign, Urbana, IL 61801 (corresponding author). E-mail: olsons@uiuc.edu

Note. This manuscript was submitted on March 1, 2008; approved on December 22, 2008; published online on July 15, 2009. Discussion period open until January 1, 2010; separate discussions must be submitted for individual papers. This paper is part of the ***Journal of Geotechnical and Geoenvironmental Engineering***, Vol. 135, No. 8, August 1, 2009. ©ASCE, ISSN 1090-0241/2009/8-1070–1081/$25.00.

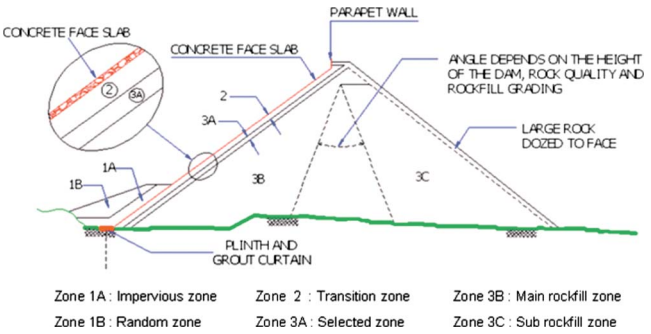

Fig. 1. Typical cross section of CFRD (Cooke and Sherard 1987)

can be related directly to an equivalent full-scale prototype, if performed under carefully controlled conditions, and have provided many practical insights to dam (or embankment) behavior under a number of loading conditions (Adalier and Sharp 2004).

In contrast, relatively few centrifuge tests have been performed on model CFRDs, despite the number of CFRDs recently constructed (Hou et al. 2004; Hou 2006; Xu et al. 2006). For example, Hou et al. (2004) performed centrifuge tests of a model CFRD with the cutoff wall and face slab connected to each other, and Xu et al. (2006) tested a model CFRD built on deep alluvium and compared the centrifuge results with numerical solutions.

In this paper, we first discuss some aspects of the current state-of-practice for monitoring CFRD performance. We then describe the rationale, materials, model design and setup, and instrumentation for a centrifuge testing program performed on a model CFRD with two different face slab stiffnesses subjected to various reservoir pool levels and compare the centrifuge results with a suite of FE analyses and with the results of field measurements made on several in-service CFRDs. Finally, we discuss critical factors affecting CFRD behavior and make suggestions for obtaining better centrifuge test results.

Typical Deformation Pattern of CFRDs

It is well known that deformations occur during construction and initial impounding of a CFRD, while after initial impounding CFRDs have historically performed well and remained stable (Materon 1985; Pinto and Marques 1998; Wu et al. 2000b). Crest settlement and face deflection are two parameters commonly used to quantify the deformation characteristics and performance of CFRDs. Several investigators (Soydemir and Kjaernsli 1979; Clements 1984; Liu et al. 1993) have proposed expressions to predict CFRD crest settlement, but this task remains difficult because numerous factors (e.g., intact particle strength, rockfill gradation, rockfill compaction, foundation conditions) affect crest settlements (Hunter and Fell 2003). For example, Fell et al. (2005) reported that both the magnitude and rate of CFRD crest settlements can vary by over one order of magnitude.

Concrete-facing deformations typically are greatest near the upper part of the slope and near the toe as a result of crest settlement and toe bulging, respectively, during construction, and near the midslope during initial impoundment (Mori 1999). Based on measured deflection distributions, CFRD face slab deflection patterns can be characterized as a *D*-shaped distribution (Li 1993) with the maximum deflection near the center of the face slab (e.g., Foz do Areia Dam) or a *B*-shaped distribution (Fitzpatrick et al. 1985; Wu et al. 2000b) with large deflections at the center of the face slab and near the top part of the slab (e.g., Cetana Dam).

Because deformation and cracking of the concrete-facing directly influence its integrity and leakage rates through CFRDs, several investigators have proposed empirical approaches to predict the magnitude of concrete-face slab deformation that results from initial impounding. However, Fell et al. (2005) reported that both the magnitude and rate of facing displacement can vary by 1–2 orders of magnitude, and are difficult to predict.

Centrifuge Model Test Program

Centrifuge Testing Program

One of the primary advantages of centrifuge modeling is that a $1/N$ scale model subjected to a gravitational acceleration of $N \times g$ (where g is acceleration of gravity) shows the same stress-strain behavior as the prototype (Schofield 1981; Adalier and Sharp 2004). Thus, the centrifuge test results can be used as a quantitative indicator of the behavior of a structure subjected to a realistic stress field, if scaling laws for the length, volume, stiffness, velocity, etc., are properly applied (Schofield 1981; Tan and Scott 1985). This study presents the results of centrifuge tests conducted at the Institute of Water Resources and Hydropower Research (IWHR) in Beijing, using their 450 g ton geotechnical centrifuge. The centrifuge is capable of reaching a maximum acceleration of $300g$ and its maximum radius is 5.0 m (Hou et al. 2004). The size of the swing basket is $1.5 \times 1.0 \times 1.2$ m ($L \times W \times H$).

The concrete-faced rockfill dam constructed for these tests was modeled after Daegok Dam, located in South Korea on the Taehwa River which flows into the East Korea Sea. Daegok Dam is a 51.8 m high and 180 m wide concrete-faced rockfill dam constructed in 2005 using locally available quarried rock, and has an upstream slope of $1V:1.4H$ (vertical:horizontal) and a downstream slope of $1V:1.8H$. Daegok Dam was constructed primarily for supplying drinking water to the metropolitan area of Ulsan, South Korea.

For the centrifuge program, we selected a scaling ratio, N, of 70 (considering the centrifuge capacity) which allowed us to model the actual dam at $1/2$ scale (i.e., prototype dimensions equal to one half of the actual dam dimensions). The centrifuge tests focused chiefly on the crest settlements and concrete-face slab deformations (using two values of face slab stiffness) when subjected to varying reservoir pool levels.

Model Preparation

Fig. 2 presents a section through the model dam and provides the model dimensions. The upstream slope ratio is $1V:1.4H$ and the downstream slope ratio is $1V:1.8H$, identical to Daegok Dam. Using a scaling factor $N=70$, the prototype dam height is 25.9 m. In each centrifuge test, the model reservoir pool was raised in five stages: 90, 155, 220, 285, and 350 mm (corresponding to 6.3, 10.9, 15.4, 20.0, and 24.5 m in prototype dimensions).

A rigid-wall model container with dimensions of $1{,}335 \times 740 \times 685$ mm ($L \times W \times H$) was used to build the model dam and house the water tank used to control the reservoir level during the tests (Fig. 3). The portion of the reservoir control system within the model container occupied a width of 340 mm, leaving a width of 400 mm for constructing the model dam.

At a scaling factor of 70, it is nearly impossible to properly model the bending stiffness of the prototype concrete using con-

J. Geotech. Geoenviron. Eng., 2009, 135(8): 1070-1081

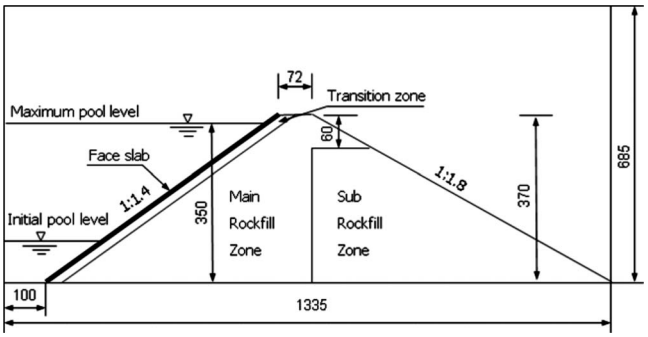

Fig. 2. CFRD model for centrifuge test (units: mm)

crete; therefore aluminum plate or epoxy fiber plate often are utilized to model prototype concrete-face slabs in centrifuge studies (Hou et al. 2004; Xu et al. 2006). In this study, we opted to use fiberglass plate to model the prototype concrete slabs. The fiberglass plate consisted of multiple layers of epoxy fiberglass cloth bonded using epoxy resin and compressed under high pressure. The thickness of each layer of the fiberglass cloth was about 0.1 mm. Compared to aluminum plates, the main advantage of the fiberglass plate is that it can be easily processed into a thin layer and handled without breakage during model preparation and setup.

The bending stiffness of model face slab is calculated as (Schofield 1980; Taylor 1995)

$$E_m^f I_m^f = \frac{(EI)_p^c}{N^3} \tag{1}$$

where E=elastic modulus (F/L^2); I=moment of inertia per unit width (L^4/L); EI=bending stiffness per unit width ($F \cdot L^2/L$); N=scaling factor; f=fiberglass plate; m=model; c=concrete; and p=prototype. We assumed that E_p^c=28 GPa. The density of fiberglass plates used ranged from 17.5 to 18.4 kN/m^3, tensile strength ranged from 245 to 343 MPa, and elastic modulus ranged from 17 to 21 GPa, yielding an average E_m^f=19 GPa.

For a prototype concrete slab with dimensions of 44.6 × 28.0 × 0.3 m ($L \times W \times$ thickness), the prototype bending stiffness is 617 t m^2/m, which corresponds to a model bending stiffness of 180 kg cm^2/cm (Table 1). Based on this model bending stiffness and the measured modulus for the fiberglass plate, the required plate thickness was 2.0 mm. For the second experiment, a 1.5 mm thick face slab was employed to model a face slab with a smaller

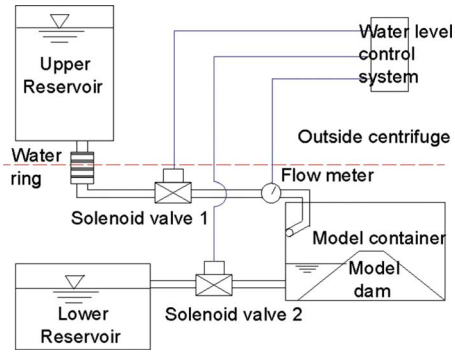

Fig. 3. Reservoir control system schematic

Table 1. Bending Stiffness and Thickness of Model Fiberglass Plate Used for Centrifuge Models

Model	$(EI)_p^c$ (t m^2/m)	$E_m^f I_m^f$ (kg cm^2/cm)	Thickness of fiberglass plate (mm)
1	617	180	2.0
2	343	100	1.5

bending stiffness. For each test, the model slab was cut into two 200 mm wide parts (corresponding to a prototype width of 14 m) to ease handling and placement.

Materials Used in Centrifuge Model Tests

The model CFRD consisted of three types of rockfill material: the main rockfill, the sub rockfill, and the transition material (Fig. 2). In centrifuge testing, many investigators prefer to use the prototype soil in the model so that the stress-strain behavior (as well as some other index and engineering properties) of the model soil matches that of the prototype. However, the large particle sizes used at Daegok Dam could not be used in the centrifuge model because of the limited container size, making it necessary to reduce the grain size of the fill materials for model construction. The similar particle distribution method (SPDM), or parallel gradation method, is widely used for this purpose. SPDM reduces the individual grain sizes while maintaining the same uniformity coefficient (C_u) and coefficient of curvature (C_c) between the prototype and mode1 soils (Lowe 1964; Ramamurthy and Gupta 1986). However, Hou et al. (2004) indicated that this method may change the engineering properties of the rockfill, particularly if it requires increasing the fines content of the model soil.

Alternatively, the equal quantity replacing method (EQRM) (Hou et al. 2004) can be used to reduce the coarser grain sizes of the model soil (i.e., C_u and C_c are changed) without significantly changing its engineering properties. In the EQRM, the finer grain sizes of the prototype soil are retained, while the coarser grain sizes are reduced based on the maximum particle size allowance of the model container.

In this study, the EQRM was applied to reduce the maximum particle size of the prototype main and sub rockfill from 600 and 300 mm, respectively, to 60 mm while retaining particles finer than 5 mm to avoid significant changes to the engineering properties of the fills. This method also maintained some differences between the main and sub rockfill materials. The maximum grain size of 60 mm was selected to be about 1/7 of the available container width of 400 mm. In contrast, the SPDM was applied for the transition fill using a reduction factor of ten in order to maintain a constant ratio of $(D_{\max})_{\text{main rockfill}}/(D_{\max})_{\text{transition fill}}$ between the prototype and the model. Fig. 4 presents the grain size distributions of the prototype and model rockfills (i.e., main, sub, and transition). The model fill materials were obtained from a quarry site in China.

To characterize their strength and stiffness, we performed drained triaxial compression tests on the model main and sub rockfills in an oversized triaxial device. Each rockfill specimen was wetted to 3–4% moisture content, thoroughly mixed, and reconstituted in a large triaxial specimen mold (300 mm diameter × 700 mm high). The specimens were prepared by placing the rockfill in five layers of approximately equal thickness. Each layer was compacted using a vibrator until a target dry density of 21.1 kN/m^3 was achieved (Varadarajan et al. 2003). The specimens were saturated by percolating water upward from the

J. Geotech. Geoenviron. Eng., 2009, 135(8): 1070-1081

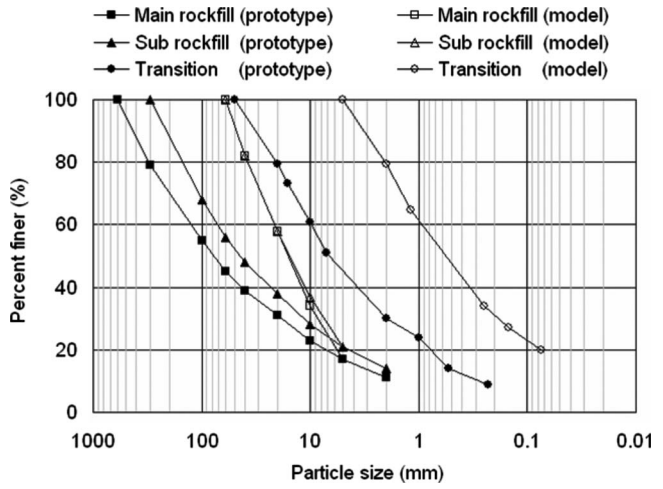

Fig. 4. Grain size distributions of prototype and model fill materials

bottom and applying a back pressure of 100 kPa (Indraratna et al. 1993), consolidated to equal all-around stresses of 0.4, 0.8, 1.2, and 1.6 MPa, and sheared at a constant rate of 2 mm/min to an axial strain of 15%. Membrane penetration during the test was minimized by using a thick membrane.

Fig. 5 presents the stress-strain-volume change behavior for the main and sub rockfill materials. Peak strengths were mobilized at intermediate strain levels that increased with increasing consolidation stress, and the postpeak response of the two materials are characterized by a nearly constant deviator stress. At lower values of consolidation stress, specimens exhibit mild volumetric dilation (following an initial volumetric contraction), which is more dominant for the main rockfill. At higher consolidation stresses, volumetric contraction is observed over a wide range of axial strains.

Fig. 5(c) presents the Mohr circles of stress for the main and sub rockfills. As anticipated, the drained friction angle for the rockfill materials decreases with increasing consolidation stress from approximately 49° at low normal stresses to 41° at a normal stress of 3 MPa. These values agree well with drained friction angles measured for other gravels and rockfills (Terzaghi et al. 1996). Fig. 5(d) presents the initial tangent drained modulus values (E_i) obtained from the triaxial tests. The measured modulus values compare favorably with values recommended by Peck et al. (1974).

In contrast to the large-specimen tests performed on the main and sub rockfills, we performed consolidated-undrained triaxial compression tests on conventionally sized (38 mm diameter and 80 mm high) specimens of the model transition material. Specimens were prepared using procedures identical to those used for the rockfill, and the transition fill specimens were also compacted to a target dry density of 21.1 kN/m^3. Following specimen preparation, the specimens were placed in the triaxial cell, saturated, and back-pressured until Skempton's B value reached 0.95 or greater, consolidated to the target consolidation stresses of 0.2, 0.4, and 0.6 MPa, and sheared under undrained conditions at a rate of 0.05 mm/min. Fig. 6 presents the stress-strain-pore-water pressure response, total and effective stress Mohr circles, and initial tangent undrained modulus for the transition fill.

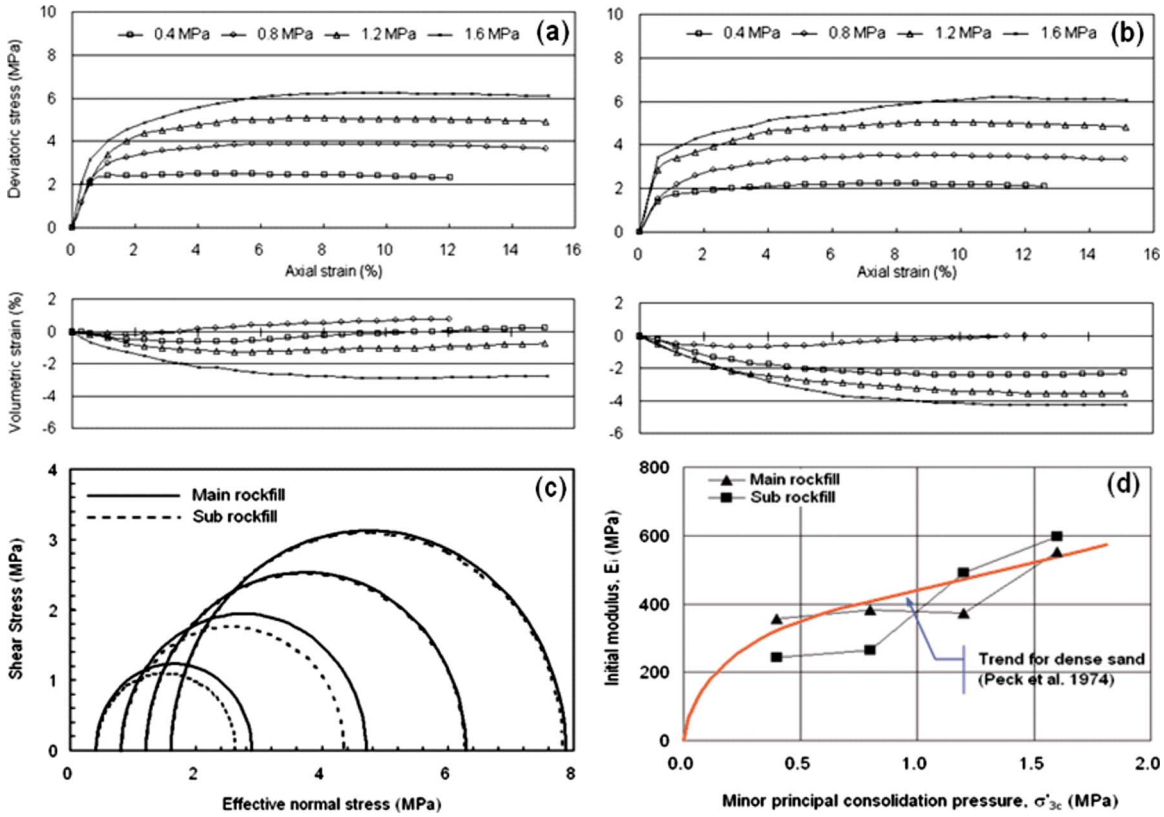

Fig. 5. Large triaxial test results on main and sub rockfill: (a) main rockfill material stress-strain and volumetric response; (b) sub rockfill material stress-strain and volumetric behavior; (c) Mohr–Coulomb failure envelope; and (d) initial tangent modulus versus minor principal consolidation stress

J. Geotech. Geoenviron. Eng., 2009, 135(8): 1070-1081

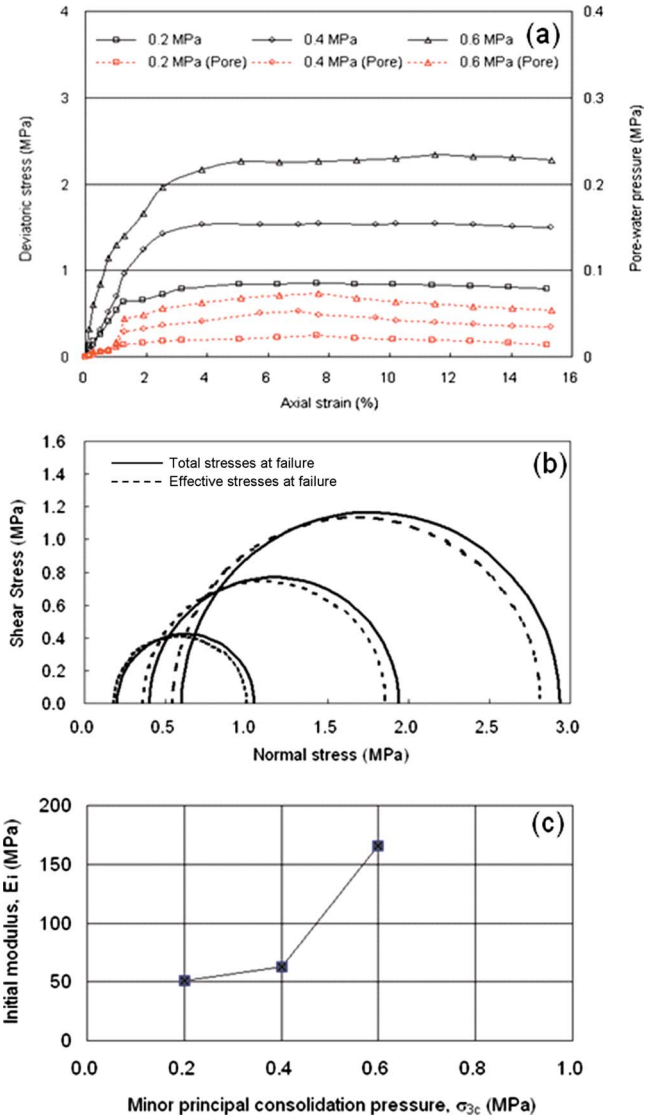

Fig. 6. Triaxial test results for transition fill: (a) stress-strain and pore-water pressure response; (b) Mohr–Coulomb failure envelope; and (c) initial modulus versus minor principal consolidation stress

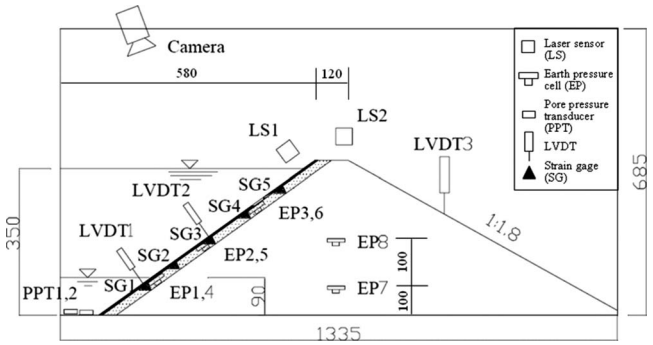

Fig. 7. Instrumentation layout of Model 1 (units: mm)

Model Construction, Instrumentation, and Testing Procedure

A four-layer steel frame for compacting the rockfill materials was manufactured to aid in keeping the density of each layer constant. After fixing the frame in the model container, rockfill materials were placed and compacted in layers to the target density of 21.1 kN/m^3. The main and sub rockfill zones were separated temporarily during model construction by a thin fiberglass plate. The 10-mm-thick transition zone was placed and compacted on the upstream slope of the dam after completing the main and sub rockfill zone construction. Finally, the fiberglass model slabs were placed above the transition zone, and the model slabs were covered with a thin rubber membrane to prevent seepage into the dam body through the spaces between the model slab sections and between the container walls and the model dam.

Instrumentation was focused on the upstream side of the dam, mainly near the model face slab, as shown in Fig. 7. One laser sensor (LS 1) and two linear variable differential transformers (LVDT 1 and LVDT 2) were installed on the upstream side, perpendicular to the model slab. Special efforts were made to ensure that LVDT 1 and LVDT 2 would work when submerged by the model reservoir, and a thin plastic plate was placed on the end of each LVDT to prevent its penetration into the rubber membrane. In Model 1, one LVDT was installed on the downstream side of the dam to measure the deformation of the downstream slope, while in Model 2, two LVDTs were installed on the downstream side to provide more detail.

The reservoir pool level was monitored using two miniature pore-water pressure transducers placed at the bottom of the reservoir. A total of eight miniature earth pressure cells were installed in each model—six along the back of the model slab (i.e., three along the centerline of each model slab section) and two along the centerline of the CFRD. The two earth pressure cells embedded in the middle of the rockfill were placed in a sand bedding and rockfill was gently compacted in their vicinity to avoid damage. Finally, five foil-type strain gages were evenly distributed along the back surface of each model face slab section (ten strain gages used per model) and a high-speed video camera was fixed at the top of the container to visually observe the dam face behavior during the tests.

Each model was spun at 70g for 4 min to reach equilibrium prior to filling the reservoir. Self-weight settlements during spin-up were reset to baseline "zero" conditions. The reservoir was filled in five stages (as indicated earlier) to model depths of 90, 155, 220, 285, and 350 mm (corresponding to prototype pool depths of 6.3, 10.9, 15.4, 20.0, and 24.5 m) while maintaining a centrifugal acceleration of 70g. Once the target reservoir stage was reached, the pool level was maintained for 5 min (which was sufficient for deformations to equilibrate). After completing the stage for the maximum pool level (350 mm), the reservoir was emptied to the minimum pool level (90 mm) at a discharge rate of 17.3 L/min.

Centrifuge Test Results and Analyses

Settlements of Dam Crest and Downstream Slope

Fig. 8 illustrates the settlements (normalized with respect to the dam height, H) at the dam crest (measured by LS 2) and downstream slopes (measured by LVDTs) in Models 1 and 2 at each reservoir pool stage. As indicated in Fig. 8, values of CFRD crest settlement of 0.17H (%) (44 mm prototype) and 0.22H (%) (57 mm prototype) were measured at the maximum reservoir pool level for Models 1 and 2, respectively. Although slightly larger crest settlements occurred in Model 2 where the face slab had a smaller bending stiffness, these factors are unlikely to be related

J. Geotech. Geoenviron. Eng., 2009, 135(8): 1070-1081

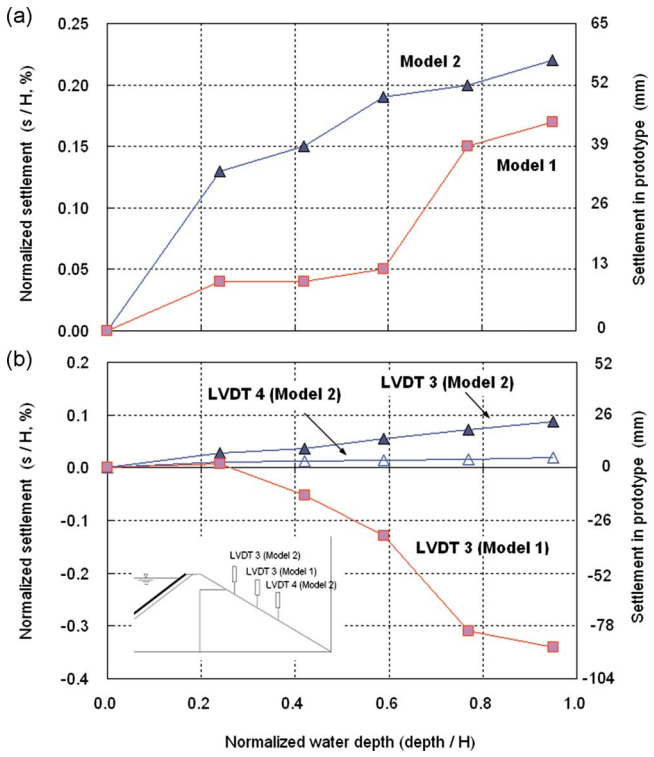

Fig. 8. Settlement for each water-level stage (s=settlement; and H =dam height); (a) dam crest; (b) downstream slope

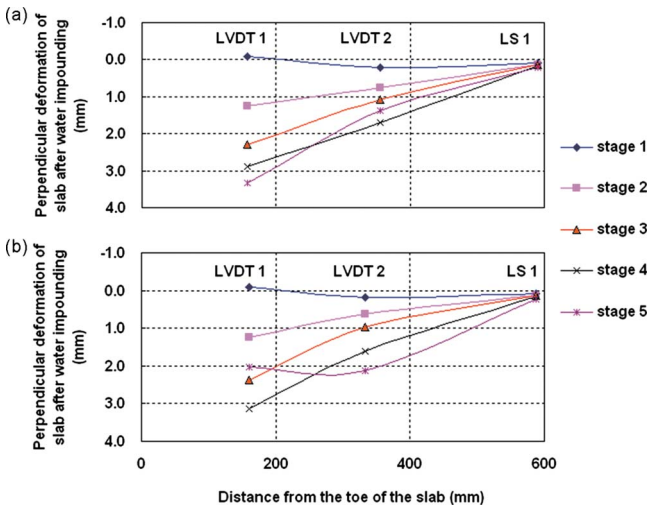

Fig. 9. Deformations of model face slabs during reservoir filling (in model dimension): (a) Model 1; (b) Model 2

because the crest settlement is related primarily to rockfill stiffness (as determined by material type, compactive effort, etc.), not the stiffness of the relatively thin face slab. However, these factors cannot be correlated in this study because of the limited number of centrifuge tests.

While the CFRD crest settlements are quite similar and exhibit similar trends, the downstream slope movements for the two models differ substantially. In Model 2, increasing settlements accompanied increasing reservoir pool level, as anticipated based on field behavior of CFRDs. In contrast, swelling occurred in Model 1 at the single downstream LVDT location, and the magnitude of swelling was approximately twice the magnitude of crest settlement. Since swelling at the middle portion of the downstream slope is rarely observed in dams (Özkuzukiran et al. 2006), we anticipate that this behavior was likely the result of minor downstream sliding or bulging of the model CFRD. This unusual behavior does not appear to reflect the different face slab stiffnesses in the two models; however, this behavior requires further study.

Deformations of Model Face Slabs

Fig. 9 presents the model face slab deformations (measured perpendicular to the face) with increasing water level. The lower two points were measured by LVDTs (LVDT 1 and LVDT 2) and the displacement near the dam crest was measured by a laser sensor (LS 1). In Model 1, face slab deformations increased with increasing reservoir pool level, and the maximum deformation was observed at the lowest point on the slab (LVDT 1). However in both models, a slightly different deformation pattern developed during the final reservoir pool stage (Stage 5). During Stage 5 in Model 2, the upstream toe of the dam appears to have swelled, suggesting that the toe of the dam bulged slightly under the maximum weight of the reservoir.

As indicated in Fig. 9, the maximum deformations during reservoir filling were 3.3 mm (23.1 cm in prototype) and 3.2 mm (22.4 cm in prototype) for Models 1 and 2, respectively, which correspond to normalized deformations of 0.90H (%) and 0.86H (%). Also as shown in Fig. 9, deformation values measured in Models 1 and 2 are almost identical, indicating that the difference in face slab bending stiffness does not significantly influence face slab deformations, at least for the range of face slab bending stiffness tested in this study.

The similar patterns of face slab deformation in the two models (with different face slab bending stiffnesses) suggest that face slab deformation is strongly influenced by the stiffness of the transition (supporting) zone below the face slab since the stiffness of the transition zone was comparable to each other. The stiffness of the main rockfill also contributes to the face slab deformation, but the initial stiffness of the rockfill (in the triaxial tests) was about five times larger (at a minor principal confining stress of 0.4 MPa) than the initial stiffness of the transition fill. We discuss the effect of the transition zone stiffness in more detail in a subsequent section.

Induced Stresses in Model Face Slabs

The stresses induced in the face slab were estimated using measurements from the strain gages attached to the back side of face slabs. Despite some difficulties in achieving reliable measurements (e.g., high accelerations induced during the centrifuge test, loss of contact between the strain gage and back of the face slab, loss of contact locally between the back of the face slab and the transition zone), the two rows of strain gages provided some redundancy in strain measurements, making it possible to discern some consistent trends with increasing water level.

Fig. 10 presents final strain distributions in the Model 1 and 2 face slabs measured at the maximum reservoir pool, as well as the maximum tensile strain measured in the face slab following each reservoir filling stage. On average, Model 1 experienced larger maximum tensile strains (0.0016% in Stage 5) than Model 2 (0.00055% in Stage 5). These strains correspond to maximum

J. Geotech. Geoenviron. Eng., 2009, 135(8): 1070-1081

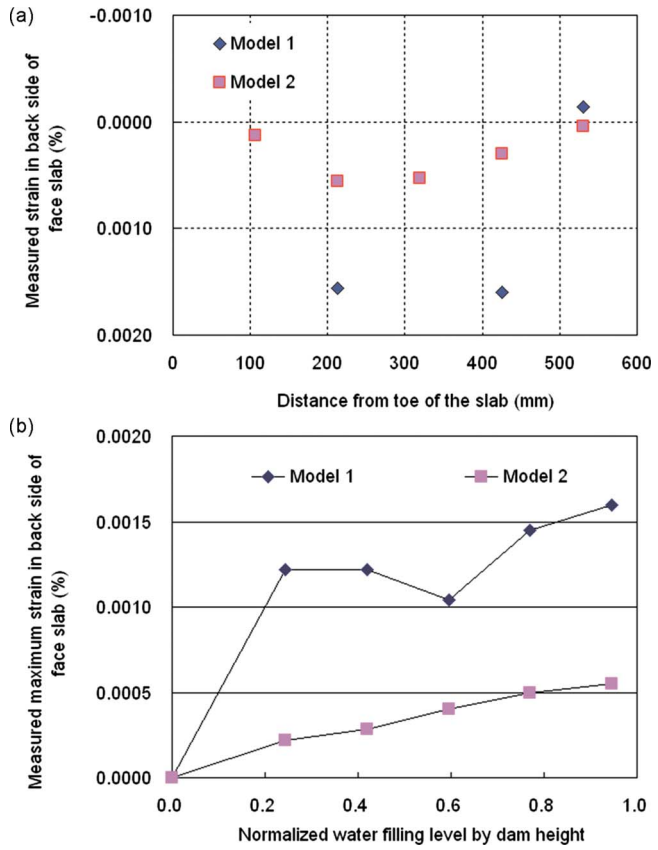

Fig. 10. Strain measurement of the face slabs (+=tensile and −=compressive): (a) final strain distribution (Stage 5); (b) measured maximum tensile strain

tensile stresses of about 0.30 and 0.10 MPa for Models 1 and 2, respectively. These results appear reasonable because both models experienced similar maximum deformations along the face, while Model 1 used a stiffer face slab. For a given face deformation, the stiffer (i.e., thicker) slab should exhibit larger strains and stresses on its surface.

We note that the limited number of displacement measurement points and limited number of reliable strain measurements make it difficult to conclusively compare the deformation patterns in Fig. 9 with the strain patterns in Fig. 10. In addition, differences in the measurement locations (for displacement and strain), potential local heterogeneity in the transition zone, lack of face slab fixity at the dam toe, and absence of displacement measurements below 160 mm from the model toe could result in discrepancies between the measured face deformations and strains on the bottom surface of the face slab. In future efforts, we recommend that these issues be carefully considered to allow direct comparisons of measured deformations and strains.

Numerical Analysis

Numerical Simulation of Centrifuge Test Results

The centrifuge tests results described above suggest that face slab stiffness (or thickness) had a negligible effect on the upstream slope deformations. We anticipate that the stiffness of the transition zone (that supports the face slab) strongly affected the face slab behavior. Numerous additional centrifuge experiments would be required to examine the effect of the transition zone stiffness. As an alternative, a parametric analysis was performed to evaluate the effect of transition zone stiffness using a numerical model that was calibrated using the measured centrifuge test results. As described subsequently, calibration was performed using an ad hoc approach by modifying soil properties (e.g., stiffness, strength) to achieve a better match between the measured and predicted results.

Table 2. Parameters Used in Material Constitutive Models for Numerical Analyses

Property	Main rockfill zone	Sub rockfill zone	Transition zone
Dry unit weight (kN/m^3)	21.1	21.1	21.1
Drained friction angle (°)	45	44	41.8
Apparent cohesion (kPa)	0	0	17
Bulk modulus (MPa)	340	323	77
Shear modulus (MPa)	157	149	35

In the numerical analyses, a Mohr–Coulomb failure criterion and constitutive model were used to simulate the behavior of the rockfill materials, i.e., main rockfill, sub rockfill, and transition zone. The input values for the Mohr–Coulomb constitutive models were derived from the laboratory triaxial compression tests, and are presented in Table 2. Values of effective stress friction angles for the main and sub rockfill materials were estimated as secant values for the average effective confining stress present in the prototype CFRD. The bulk and shear moduli were estimated using the average secant modulus measured at a displacement corresponding to 50% of the peak shear strength and an assumed Poisson's ratio of 0.3. The concrete-face slab was simulated using beam elements. Finally, the increasing reservoir pool level was simulated by applying an increasing hydrostatic pressure to the beam elements.

Fig. 11 compares face slab displacements (normal to the face surface) measured in the centrifuge tests (shown in prototype scale) to those computed for Models 1 and 2. Despite some discrepancies, the numerical analyses yield overall estimates of face

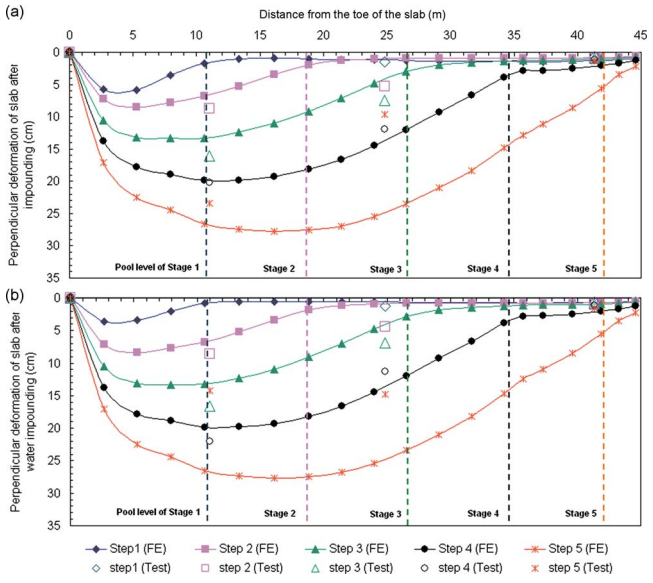

Fig. 11. Displacements normal to face slab surface from centrifuge tests and numerical analyses: (a) Model 1; (b) Model 2

J. Geotech. Geoenviron. Eng., 2009, 135(8): 1070-1081

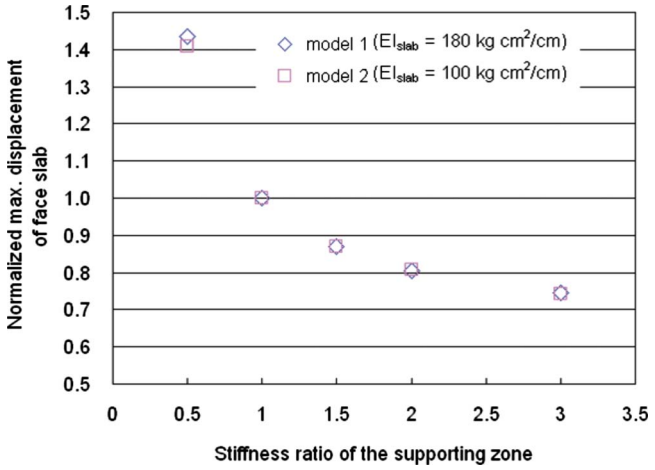

Fig. 12. Normalized maximum displacement of face slab normal to its surface against transition zone stiffness ratio

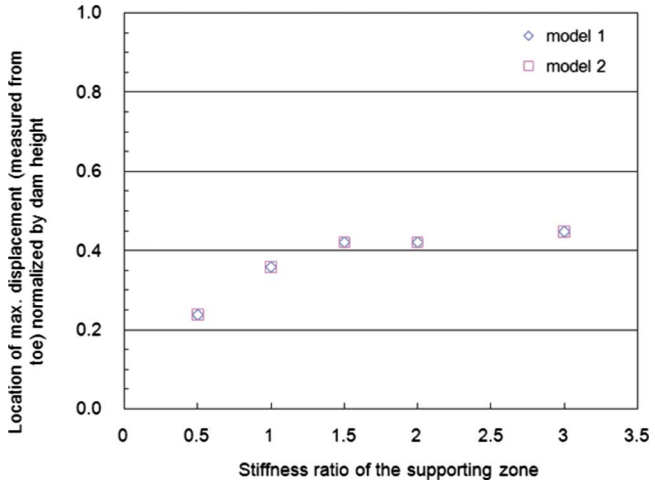

Fig. 13. Position of maximum face slab displacement as function of transition zone stiffness

slab displacement that compare reasonably well to the *D*-shaped displacement patterns measured in the centrifuge experiments. We note that the primary differences occur in the latter stages of loading in the upper part of the face slab where the centrifuge models experienced smaller displacements than predicted by the numerical analysis. Nevertheless, the maximum face slab displacements predicted by the two numerical analyses are nearly identical, suggesting that both the maximum displacement normal to face slab and the displacement pattern estimated by numerical analysis are not affected by the flexural rigidity (i.e., thickness) of the concrete-face slab.

Displacements Normal to Concrete-Face Slab Surface

Additional numerical analyses were performed to investigate the effect of varying the transition zone stiffness on the face slab displacement pattern. Specifically, we varied the transition zone stiffness by factors of 0.5, 1, 1.5, 2, and 3 times the transition zone stiffness reported in Table 2.

Fig. 12 presents the computed maximum displacements (normal to the face slab) that occur as a result of changes in transition zone stiffness. In the figure, the transition zone stiffness is characterized using the ratio of secant modulus used in the particular numerical simulation to the transition zone secant modulus used in Table 2. These results suggest that significant increases in transition zone stiffness reduce face slab displacements (albeit at a diminishing rate), but decreases in transition zone stiffness markedly increase the maximum face slab displacements (at least for the range of transition zone stiffness investigated here).

Fig. 13 presents the locations of maximum face slab deflection (normalized by dam height) computed at the maximum reservoir level as the transition zone stiffness ratio is varied. These results illustrate that the face slab flexural stiffness has a minor effect on the position of maximum deformation (normal to the face surface) as the stiffness of the transition zone increases and a slightly larger effect as the transition zone stiffness decreases considerably. As shown in the figure, the maximum displacement occurs at a position of about 40% of dam height (H) for all cases other than the lowest transition zone stiffness, consistent with field observations.

Although there will be some variation in transition zone stiffness in CFRD construction depending on material selection and compaction methods, the range of stiffness examined in the numerical study (i.e., stiffness varied by a factor of six) may be more than can be reasonably achieved in the field for a single material type. However, considering the potential variability of transition zone materials and properties that could be used for CFRD construction, the results presented in Figs. 12 and 13 provide meaningful insight regarding the impact of face slab and transition zone stiffness on CFRD behavior.

Tensile Stresses in Concrete-Face Slab

In a CFRD, the upstream concrete-face slab typically serves as the only barrier to seepage through the dam. Although piping is unlikely in most CFRDs, severe cracking can result in excessive leakage through the concrete facing, preventing the dam from properly impounding water. Concrete cracking and water infiltration can lead to corrosion of steel reinforcement and further damage to the concrete facing. Therefore, the concrete-face slab must be designed to resist tensile cracking resulting from the displacements and moments imposed by the external hydraulic loading applied by the reservoir. Giudici et al. (2000) reported that the displacements and moments in the concrete-face slab can be correlated to the face slab flexural stiffness, transition zone stiffness, and stiffness of the rockfill underlying the upstream slope.

Cracking of the concrete-face slab will occur where the tensile stresses induced in the face slab exceed its tensile strength. Fig. 14 shows the effect of transition zone stiffness on maximum tensile stresses induced in the face slab computed in the numerical analyses. The results indicate that maximum tensile stresses in the face slab primarily depend on the transition zone stiffness and secondarily on the flexural stiffness of the face slab (at least within the range of slab stiffness examined in this study). As expected, the induced tensile stresses are larger in Model 1 where the concrete-face slab is stiffer. Furthermore, these results suggest that the maximum tensile stresses can vary considerably (by a factor of almost nine) when the transition zone stiffness varies by a factor of six.

In summary, the numerical analyses suggest that the transition zone stiffness greatly affects the performance of concrete-face slabs in CFRDs, while the flexural stiffness of the slab (at least for the range of stiffness examined in this study) plays a secondary role in the magnitude of displacements, induced strains, and tensile stresses.

J. Geotech. Geoenviron. Eng., 2009, 135(8): 1070-1081

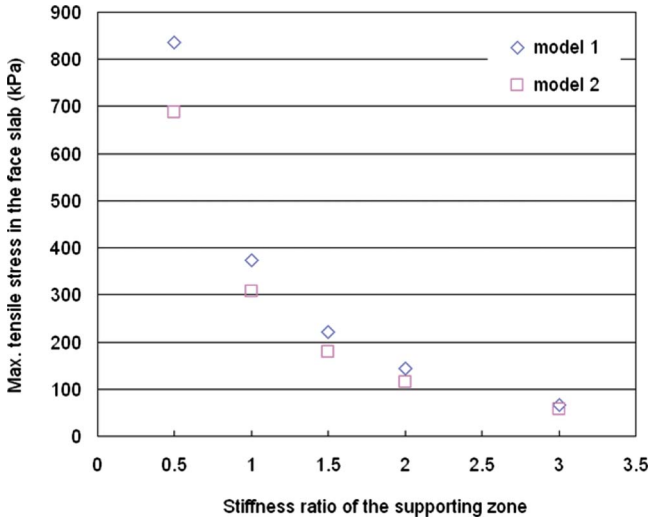

Fig. 14. Maximum tensile stresses measured in face slab as function of transition zone stiffness

CFRD Field Measurements and Comparison to Centrifuge Results

CFRD Field Measurement Data

Table 3 summarizes construction details and displacement measurements for 25 CFRDs built in Australia, Colombia, Brazil, Thailand, Sri Lanka, China, and Korea in the last 40 years. Fig. 15 presents the maximum dam crest settlements measured at these 25 CFRDs with respect to elapsed time after impounding.

Hunter and Fell (2003) and Fell et al. (2005) reported that normalized CFRD crest settlements shortly after initial reservoir filling generally range from 0.02H to 0.05H% for compacted rockfill with very high strength mineralogy, and from 0.10H to 0.15H% for compacted rockfill with intermediate to high strength mineralogy. However, as illustrated in Fig. 15, some CFRDs exhibit crest settlements considerably larger than these typical values. We note, though, that these measurements were (in many cases) made long after first reservoir filling, and therefore may

Table 3. Select Details and Deformation Measurements for 25 In-Service CFRDs

Number	Name	Country	Year	Height (m)	Length (m)	Rockfill mineralogy	Void ratio	Crest settlement (m)	Crest settlement H (%)	Face deflection (m)	Face deflection H (%)	Measuring period (year)
1	Cethana[a]	Australia	1971	110	215	Quartzite	0.26	0.18	0.16	0.17	0.16	30
2	Alto Anchicaya[b]	Colombia	1974	140	260	Hornfels	0.22	0.17	0.12	0.16	0.11	10
3	Sugaroaf[c]	Australia	1979	85	1,050	Siltstone	0.30	0.21	0.25	0.16	0.19	15
4	Foz do Areia[b]	Brazil	1980	160	828	Basalt	0.33	0.21	0.13	0.78	0.49	20
5	Mackintosh[a]	Australia	1981	75	465	Greywacke	0.24	0.24	0.32	0.25	0.33	19
6	Mangrove creek[f]	Australia	1981	80	384	Siltstone	0.26	0.08	0.10	0.10	0.13	4
7	Murchison[a]	Australia	1982	94	200	Rhyolite	0.23	0.08	0.09	0.09	0.10	17
8	Bastyan[c]	Australia	1983	75	430	Rhyolite	0.23	0.05	0.07	0.07	0.09	8
9	Khao Laem[d]	Thailand	1984	113	910	Limestone	0.29	0.19	0.17	0.13	0.12	14
10	Shiroro[c]	Nigeria	1984	125	560	Granite	0.20	0.17	0.14	0.09	0.07	2
11	Dongbok[e]	Korea	1985	45	188	Andesite	0.27	0.04	0.09	0.04	0.09	7
12	Lower Pieman[a]	Australia	1986	122	360	Dolerite	0.24	0.22	0.18	0.27	0.22	14
13	Chengbing[h]	China	1989	75	325	Tuff lava	0.28	0.10	0.13	0.19	0.25	10
14	Xibeikou[c]	China	1989	95	222	Limestone	0.28	0.06	0.06	0.08	0.08	7
15	Segredo[b]	Brazil	1993	145	705	Basalt	0.37	0.23	0.16	0.34	0.23	8
16	Xingo[c]	Brazil	1994	150	850	Granite	0.28	0.53	0.35	0.51	0.34	6
17	Tianshenqiao[g]	China	1999	178	1,168	Limestone	0.31	1.06	0.60	1.14	0.64	1.5
18	Ita[c]	Brazil	1999	125	880	Basalt	0.31	0.60	0.48	0.46	0.37	3
19	Namgang[e]	Korea	2001	34	1,126	Gneiss	0.27	0.01	0.04	0.06	0.17	6
20	Yongdam[e]	Korea	2001	70	498	Schist	0.32	0.12	0.17	0.01	0.01	6
21	Miryang[e]	Korea	2001	89	535	Granite	0.18	0.09	0.10	0.16	0.18	6
22	Sancheong(L)[e]	Korea	2002	71	286	Granite	0.27	0.09	0.13	0.01	0.01	4
23	Sancheong(U)[e]	Korea	2002	87	360	Gneiss	0.27	0.30	0.34	0.01	0.01	4
24	Jangheung[e]	Korea	2005	53	403	Tuff	0.28	0.02	0.04	0.03	0.06	1
25	Daegok[e]	Korea	2005	52	190	Gneiss	0.25	0.02	0.04	0.01	0.02	1

[a]Giudici et al. (2000).
[b]He (2000).
[c]Hunter (2003).
[d]Kashiwayanagi et al. (2000).
[e]Kwater (2005).
[f]Mackenzie and McDonald (1985).
[g]Wu et al. (2000a).
[h]Wu et al. (2000b).

J. Geotech. Geoenviron. Eng., 2009, 135(8): 1070-1081

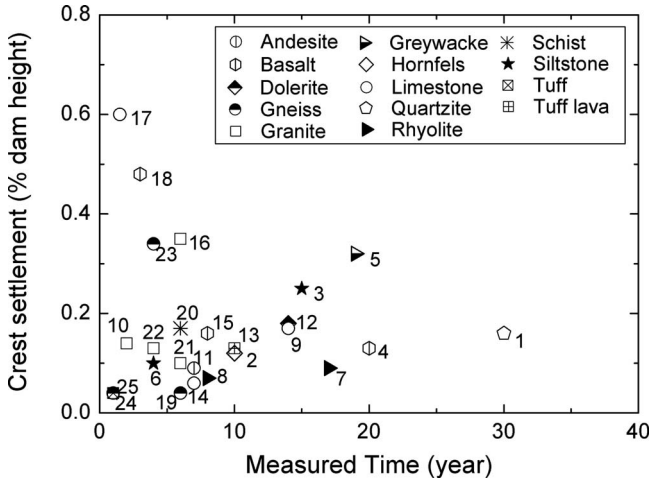

Fig. 15. Maximum CFRD crest settlements with respect to measuring period after impounding (with rockfill mineralogy highlighted); number beside data point indicates case record

include components of foundation settlement and/or secondary compression of the rockfill (i.e., long-term creep).

It is noteworthy that over half of these cases exhibited crest settlements of 0.15H% or smaller, but some of the CFRDs such as Xingo Dam (0.35H%), Ita Dam (0.48H%), and Tianshenqiao Dam (0.60H%) have exhibited relatively large settlements. Such large settlement may be the result of both the low rockfill modulus (Xingo: E_v=32 MPa) and large heights (Tiashenqiao: H =178 m). We anticipate that the large settlements experienced by some CFRDs shortly after reservoir filling may be related to dam height, rockfill characteristics (i.e., low strength mineralogy or weak, crushable particles; poorly graded particle size distribution; presence of fines in the rockfill), construction and/or compaction methods, and foundation characteristics (i.e., thickness and compressibility of alluvium, excessive bedrock jointing), among other factors. Accordingly, these factors should be considered to improve CFRD crest settlement predictions.

Fig. 16 presents maximum CFRD face slab deflections (normalized by dam height) with time after reservoir filling. From

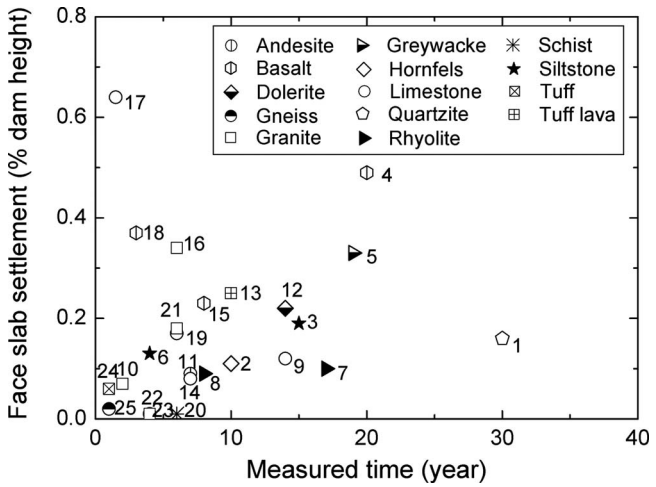

Fig. 16. Maximum face slab deflection of CFRD with respect to measuring period after impounding (with rockfill mineralogy highlighted); number beside data point indicates case record

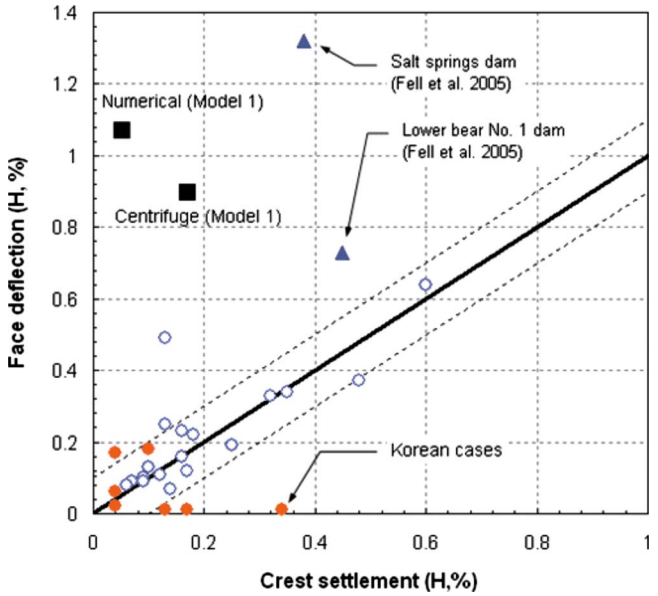

Fig. 17. Comparison of crest settlements and maximum face deflections for CFRDs in Table 3, centrifuge test results for Model 1, and numerical analysis of Model 1

measurements of CFRD deformations in Australia, Fitzpatrick et al. (1985) reported that face slab deflections generally were about 60% of the crest settlements, and that the average deformation rate during the first 10 years following impoundment was approximately 3 mm/year.

In Fig. 16, nearly all of the normalized face slab deflections are less than 0.4H%, and over half exhibit values less than 0.2H%. However, a small percentage of CFRDs exhibited large maximum face slab deformations, such as Tianshenqiao Dam (0.64H%) and Foz Do Areia Dam (0.49H%). These large face slab deflections likely result from the same factors that lead to large crest settlements, as well as the transition zone characteristics (e.g., gradation, thickness, and compaction).

Fig. 17 compares measured crest settlements to maximum face slab deformations. Based on the field measurements, crest settlements are (on average) approximately equal to maximum face slab deformations, and over 70% of the measurements fall within bounds shown in the plot. Fig. 17 includes two additional cases reported by Fell et al. (2005) of CFRDs constructed using dumped and sluiced rockfill, differing from the placement and compaction methods used for the modern dams reported in Table 3.

Comparison of Field Measurements, Centrifuge Test Results, and Numerical Analyses

Fig. 17 also compares the centrifuge experiment and numerical analysis result to the CFRD field data, focusing on in-service CFRDs constructed in Korea in the last 6 years (Cases 19–25). As illustrated in the figure, the centrifuge experiments exhibited crest settlements (average of 0.19H%) similar to the Korean case histories (average of 0.12H%). This result indicates that centrifuge modeling can reasonably approximate the crest settlements of CFRDs.

In contrast, the centrifuge models exhibited considerably larger maximum face slab deflections (average of 0.88H%) than measured in the Korean cases (average of 0.07H%). The centri-

J. Geotech. Geoenviron. Eng., 2009, 135(8): 1070-1081

fuge model face slab deflections also greatly exceeded nearly all of the field data, excluding the cases reported by Fell et al. (2005) that were constructed using dumped and sluiced rockfill. The large values measured in the centrifuge may be attributed to experimental limitations, such as: (1) difficulty in compacting the outer portion of upstream slope as a result of the compaction mold configuration; (2) lack of constraint on the lower part of the model face slab (i.e., incomplete fixity at the toe); (3) differences in the model face slab/transition zone interface compared to field conditions; (4) an overly simplified installation process for the model face slabs; and (5) differences in rockfill gradation.

From these comparisons, it appears that the centrifuge models are capable of providing crest settlements comparable to field CFRD measurements. While the face slab deflections are larger than those generally observed in the field, some modifications to the model design and construction should improve the centrifuge model performance and provide maximum face slab deflections that agree better with in-service CFRDs constructed with compacted rockfill.

Similarly, the numerical models reasonably predicted the crest settlements, but greatly overestimated the maximum face slab deflections. The reasons for this are likely twofold. First, the numerical model was calibrated using the centrifuge experiment data, and as a result, reasonably mimic the centrifuge results (which also greatly overestimated the maximum face slab deflections). Second, and perhaps more importantly, the numerical model utilized in this study was a fairly simple two-dimensional model. In order to more accurately assess the face slab deflections (as well as the stresses within the face slab), it is likely necessary to develop a three-dimensional numerical model that incorporates the interaction between the different elements of a CFRD (i.e., plinth, curb, concrete-face slabs/joints, and rockfill), as well as the size and shape of the valley (C. Marulanda, written communication, 2008).

Conclusions

Centrifuge tests were performed to investigate the behavior of CFRDs with two different face slab stiffnesses when subjected to various reservoir pool levels. The CFRD scale models were based on a 1/2-scale prototype of Daegok Dam in Korea, following appropriate centrifuge scaling laws. The centrifuge test results are compared with FE analyses and with the results of field measurements made on several in-service CFRDs.

The centrifuge models with different face slab stiffnesses experienced nearly identical magnitudes of both crest settlement and maximum face slab deformation, implying that differences in face slab bending stiffness does not significantly influence CFRD deformations during reservoir filling, at least for the range of face slab bending stiffness examined here. In future studies, we recommend that a wider range of face slab stiffness be tested to evaluate its role on the upstream slope deflection pattern. As expected, for a given face slab deformation, the model with the stiffer slab exhibited larger strains and stresses.

To examine the effect of transition zone stiffness, a parametric study was performed using a numerical (FE) model that was calibrated using the measured centrifuge test results. The input values for the constitutive models used in the numerical analyses were derived from a series of laboratory triaxial compression tests performed on the materials used to construct the centrifuge models. In the parametric study, the transition zone stiffness was varied by factors of 0.5, 1, 1.5, 2, and 3 times the original transition zone stiffness. The numerical analyses revealed that the transition zone stiffness significantly affected the maximum face slab displacement, location of the maximum displacement, and tensile stresses in the face slab.

Deformation measurements for 25 in-service CFRDs constructed in the last 40 years are presented and compared with the centrifuge model deformations. The centrifuge experiments exhibited crest settlements similar to those experienced by the Korean CFRDs, suggesting that centrifuge modeling can reasonably approximate field crest settlement of CFRDs. However, the centrifuge models exhibited considerably larger maximum face slab deflections than the Korean CFRDs, and larger than all but a few in-service CFRDs examined here. The larger face slab deformations measured in the centrifuge test likely resulted from some experimental limitations, such as: (1) difficulty in compacting the outer portion of upstream slope as a result of the compaction mold configuration; (2) lack of constraint on the lower part of the model face slab (i.e., incomplete fixity at the toe); (3) differences in the model face slab/transition zone interface compared to field conditions; (4) an overly simplified installation process for the model face slabs; and (5) differences in rockfill gradation. The difficulty in achieving proper compaction along the outer portion of the slopes at model scale (where the dimensions and confining pressures are small) may have had the largest effect and should be further investigated.

Based on our examination of in-service CFRDs and the work of other investigators, deformations resulting from reservoir filling are strongly influenced by dam height, rockfill characteristics (i.e., mineralogy, gradation, presence of fines in the rockfill), construction and compaction methods, and foundation characteristics (i.e., thickness and compressibility of alluvium, excessive bedrock jointing). Accordingly, these factors should be considered to improve CFRD crest settlement predictions. Centrifuge tests can provide useful insights on the actual behavior of CFRDs and can be used to calibrate numerical models. In future studies, if some of the limitations encountered in this study are addressed, the use of centrifuge models for simulating CFRD behavior can be improved and extended to a variety of purposes.

Acknowledgments

The writers would like to thank the editor, Dr. Camilo Marulanda, and two anonymous reviewers for their constructive criticism of the manuscript. Their efforts improved the quality of the paper.

References

Adalier, K., and Sharp, M. K. (2004). "Embankment dam on liquefiable foundation-dynamic behavior and densification remediation." *J. Geotech. Geoenviron. Eng.*, 130(11), 1214–1224.

Al-Hussaini, M. M., Goodings, D. J., Schofield, A. N., and Townsend, F. C. (1981). "Centrifuge modeling of coal waste embankments." *J. Geotech. Engrg. Div.*, 107, 481–499.

Clements, R. P. (1984). "Post-construction deformation of rockfill dams." *J. Geotech. Engrg.*, 110(7), 821–840.

Cooke, J. B. (1984). "Progress in rock-fill dams." *J. Geotech. Engrg.*, 110(10), 1381–1414.

Cooke, J. B., and Sherard, J. L. (1987). "Concrete-face rockfill dam. II: Design." *J. Geotech. Engrg.*, 113(10), 1113–1132.

Fahey, M., and Katagiri, M. (1994). "Centrifuge modeling of spontaneous liquefaction of tailings dam." *Proc., Japan Earthquake Engineering Symposium*, 9(3), 271–276.

Fell, R., MacGregor, P., Stapledon, D., and Bell, G. (2005). *Geotechnical engineering of dams*, Balkema, Rotterdam, The Netherlands.

Fitzpatrick, M. D., Cole, B. A., Kinstler, F. L., and Knoop, B. P. (1985). "Design of concrete-faced rockfill dams." *Concrete face rockfill dams—Design, construction, and performance*, J. B. Cooke and J. L. Sherard, eds., ASCE, New York, 410–434.

Giudici, S., Herweynen, R., and Quinlan, P. (2000). "HEC experience in concrete faced rockfill dams." *Proc., Int. Symp. on Concrete Faced Rockfill Dams*, International Committee on Large Dams, Beijing, 29–46.

He, G. (2000). "Technical study on crest overflow of concrete faced rockfill dams." *Proc., Int. Symp. on Concrete Faced Rockfill Dams*, International Committee on Large Dams, Beijing, 283–291.

Hou, Y. J. (2006). "Study of underwater density after riprap construction with geo-centrifuge." *Proc., Int. Physical Modeling in Geotechnics ICPMG '06*, C. W. W. Ng, Y.-H. Wang, and L. M. Zhang, eds, Taylor and Francis Group, London, 425–429.

Hou, Y. J., Xu, Z. P., and Liang, J. H. (2004). "Centrifuge modeling of cutoff wall for CFRD built in deep overburden." *Proc., Int. Conf. of Hydropower*, Yichan, China, 86–92.

Hunter, G. (2003). "The pre- and post-failure deformation behavior of soils slopes." Ph.D. thesis, Univ. of New South Wales, New South Wales, Australia.

Hunter, G., and Fell, R. (2003). "Rockfill modulus and settlement of concrete face rockfill dams." *J. Geotech. Geoenviron. Eng.*, 129(10), 909–917.

Indraratna, B., Wijewardena, L. S. S., and Balasubramaniam, A. S. (1993). "Large-scale triaxial testing of greywacke rockfill." *Geotechnique*, 42(1), 37–51.

Jiang, G., and Cao, K. (1993). "Concrete face rockfill dams in China." *Proc., Int. Symp. on High Earth-Rockfill Dams*, Vol. 3, Beijing, 25–37.

Jiang, G. C., and Zhao, Z. K. (2000). "High rise CFRD in China." *Proc., Int. Symp. on Concrete Faced Rockfill Dams*, International Committee on Large Dams, Beijing, 1–17.

Kashiwayanagi, M., Koizumi, S., Ishimura, Y., and Kakiage, H. (2000). "A fundamental study on the face slab joint behavior of the CFRD." *Proc., Int. Symp. on Concrete Faced Rockfill Dams*, International Committee on Large Dams, Beijing, 341–349.

Koushige, N., Okumura, T., Narita, K., and Murase, Y. (1995). "Centrifuge model tests on hydraulic fracturing in fill-type dams." *Proc., Annual Conf. of the JSCE*, 50, 834–835.

Kwater. (2005). "Dam integration information system." *Technical rep.*, Korea Water Resources Corporation, Korea.

Li, Z. (1993). "Deformation observation on Longxi concrete face rockfill dam." *Proc., Int. Symp. on High Earth-Rockfill Dams*, Vol. 2, Beijing, 514–521.

Liu, F., Chen, Y., Liu, J., and Ni, Y. (1993). "Construction materials selection and characteristics of Wan An Xi concrete raced rockfill dam." *Proc., Int. Symp. on High Earth-Rockfill Dams*, Beijing, 272–285.

Lowe, J. (1964). "Shear strength of coarse embankment dam materials." *Proc., 8th Int. Congress on Large Dams*, Vol. 3, 745–761.

Mackenzie, P. R., and McDonald, L. A. (1985). "Mangrove Creek dam: Use of soft rock for rockfill." *Concrete face rockfill dams-design, Construction, and performance*, J. B. Cooke and J. L. Sherard, eds., ASCE, New York, 208–230.

Materon, B. (1985). "Alto Anchicaya dam—Ten years performance." *Concrete face rockfill dams—Design, construction, and performance*, J. B. Cooke and J. L. Sherard, eds., ASCE, New York, 73–86.

Mikasa, M., Mochizuki, A., and Matumoto, T. (1981). "Stability tests of a rockfill dam by centrifuge." *Proc., 10th Int. Conf. on Soil Mechanics and Foundation Engineering*, Vol. 3, 475–478, Oslo, Norway.

Mori, R. T. (1999). "Deformation and cracks in concrete face rockfill dams." *Proc., 2nd Symp. on Concrete Face Rockfill Dams*, Brazilian Committee on Dams, Florianopolis, Brazil, 49–61.

Özkuzukiran, S., Özkan, M. Y., Özyazicioğlu, M., and Yildiz, G. S. (2006). "Settlement behavior of a concrete faced rock-fill dam." *Geotech. Geologic. Eng.*, 24, 1665–1678.

Peck, R. B., Hanson, W. E., and Thornburn, T. H. (1974). *Foundation engineering*, 2nd Ed., Wiley, New York.

Pinto, N. L. S., and Marques, F. P. (1998). "Estimating the maximum face deflection in CFRDs." *Int. J. Hydropow. Dams*, 5(6), 28–31.

Ramamurthy, T., and Gupta, K. K. (1986). "Response paper to how ought one to determine soil parameters to be used in the design of earth and rockfill dams." *Proc., Indian Geotechnical Conf.*, Vol. 2, New Delhi, India, 15–19.

Rechard, R. P., and Sutherland, H. J. (1984). "Centrifuge simulations of stable tailings dam." *J. Geotech. Engrg.*, 110(3), 390–402.

Schofield, A. N. (1980). "Cambridge University geotechnical centrifuge operation, Rankine lecture." *Geotechnique*, 30(3), 227–268.

Schofield, A. N. (1981). "Dynamic and earthquake geotechnical centrifuge modeling." *Proc., Int. Conf. on Recent Advances in Geotechnical Earthquake Eng., and Soil Dynamics*, 3, 1081–1100, St. Louis, Mo.

Soydemir, C., and Kjaernsli, B. (1979). "Deformation of membrane-faced rockfill dams." *Proc., 7th European Conf. on Soil Mechanics and Foundation Engineering*, British Geotechnical Society, Brighton, East Sussex, England.

Tan, T. S., and Scott, R. F. (1985). "Centrifuge scaling considerations for fluid particle systems." *Geotechnique*, 35(4), 461–470.

Taylor, R. N. (1995). "Centrifuge in modelling: principles and scale effects." *Geotechnical centrifuge technology*, Blackie Academic and Professional, Glasgow, U.K., 19–33.

Terzaghi, T., Peck, R. B., and Mesri, G. (1996). *Soil mechanics in engineering practice*, 3rd Ed., Wiley, New York.

Varadarajan, A., Sharma, K. G., Venkatachalam, K., and Gupta, A. K. (2003). "Testing and modeling two rockfill materials." *J. Geotech. Geoenviron. Eng.*, 129(3), 206–218.

Wu, G. Y., Freitas, M., S., Jr., Araya, J. A. M., Huang, Z. Y., and Mori, R. T. (2000a). "Tianshengqiao-1 CFRD monitoring & performance lessons & new trends for future CFRDs (CHINA)." *Proc., Int. Symp. on Concrete Faced Rockfill Dams*, International Committee on Large Dams, Beijing, 573–585.

Wu, H., Wu, J., Wang, S., Wu, Q., and Cao, K. (2000b). "Ten years surveilance of Chengbing concrete face rockfill dam." *Proc., Int. Symp. on Concrete Faced Rockfill Dams*, International Committee on Large Dams, Beijing, 595–605.

Xing, H. F., Gong, X. N., Zhou, X. G., and Fu, H. F. (2006). "Construction of concrete faced rockfill dams with weak rocks." *J. Geotech. Geoenviron. Eng.*, 132(6), 778–785.

Xu, Z., Hou, Y. J., Liang, J., and Han, L. (2006). "Centrifuge modeling of concrete faced rockfill dam built on deep alluvium." *Proc., 6th Int. Conf. Physical Modeling in Geotechnics*, C. W. W. Ng, Y.-H. Wang, and L. M. Zhang, eds., Taylor & Francis Group, London, 435–440.

Zhang, L., and Hu, T. (1994). "Evaluation of the cut-off structures of rockfill dams." *Proc., Centrifuge '94*, Leung, Lee, and Tan, eds., Balkema, Rotterdam, The Netherlands, 593–598.

J. Geotech. Geoenviron. Eng., 2009, 135(8): 1070-1081